Journal of Power Sources 195 (2010) 1640–1646

Contents lists available at ScienceDirect

Journal of Power Sources

journal homepage: www.elsevier.com/locate/jpowsour

Highly efficient CO_2 bubble removal on carbon nanotube supported nanocatalysts for direct methanol fuel cell

Soon-Lin Chen[a,*], Chun-Ting Lin[a], Ching-Chang Chieng[a], Fan-Gang Tseng[a,b,*]

[a] Department of Engineering and System Science, National Tsing Hua University, Hsinchu, 30043, Taiwan
[b] Division of Mechanics, Research Center for Applied Sciences, Academia Sinica, Taiwan

ARTICLE INFO

Article history:
Received 21 July 2009
Received in revised form
22 September 2009
Accepted 30 September 2009
Available online 7 October 2009

Keywords:
Direct methanol fuel cell
Carbon nanotubes
Carbon dioxide microbubbles

ABSTRACT

In this paper, we investigate the CO_2 microbubble removal on carbon nanotube (CNT)-supported Pt catalysts in direct methanol fuel cells (DMFCs). The experiments involve the incorporation of near-catalyst-layer bubble visualization and simultaneous electrochemical measurements in a DMFC anodic half cell system, in which CH_3OH electro-oxidation generate carbon dioxide (CO_2) microbubbles. We observe rapid removal of smaller CO_2 bubble sizes and less bubble accumulation on a Pt-coated CNT/CC (Pt/CNT/CC, CC means carbon cloth) electrode. The improved half cell performances of the high CO_2 microbubble removal efficiency on the CNT-modified electrode (Pt/CNT/CC) were 34% and 32% higher than on Pt/CC and Pt/CP electrodes, respectively.

1. Introduction

Assisting or even replacing secondary batteries with fuel cells has been a research goal in recent years [1,2]. Since methanol has a higher energy density under ambient conditions and can be processed and stored more easily than a gas fuel, liquid-fed direct methanol fuel cells (DMFCs) are potential power sources for portable applications [3,4]. In a direct methanol fuel cell, the reaction of the methanol fuel is as follows:

$$\text{Anode}: \quad CH_3OH + H_2O \rightarrow CO_2 + 6H^+ + 6e^- \tag{1}$$

$$\text{Cathode}: \quad 6H^+ + 6e^- + 1.5O_2 \rightarrow 3H_2O \tag{2}$$

$$\text{Totalreaction}: \quad CH_3OH + 1.5O_2 \rightarrow CO_2 + 2H_2O \tag{3}$$

In the development of micro-DMFCs, the growth and detachment of the by-product, CO_2 microbubbles, is very important in anode reaction chamber design. The reactants (methanol and water) are in the liquid phase, so when CO_2 microbubbles cannot be effectively removed, they will accumulate on the catalyst surface and reduce the working efficiency. Scott et al. [5] investigated the removal of gas from a parallel channel and a dotted channel, and found that fuel can enter electrodes and carbon dioxide can be removed more easily on dotted channels because of the Teflon coating on the carbon cloth helping to separate the liquid flow from the gas flow. The non-Teflonized cloth produced the poorest performance of all of the electrodes. Increasing the Teflon content up to 20% improved cell performance up to current densities of 160 mA cm^{-2}. Lu and Wang [6] also found that smaller and more uniformly sized bubbles could be formed on hydrophilic carbon cloth. Bewer et al. [7] adopted oxygen bubbles generated by hydrogen peroxide on a platinum catalyst to imitate carbon dioxide bubbles on various channels. They found that for hydrogen peroxide solutions at the proper concentration (1–6%, vol.%), the quantity of the oxygen produced was comparable to the carbon dioxide generated from methanol in a DMFC; thus, a hydrogen peroxide system can be utilized to imitate the carbon dioxide bubbles generated in a fuel cell. This approach provides a model for the flow patterns in DMFCs by using simple low-cost hardware. Scott et al. [8] compared the bubble removal abilities of different carrier plates and found that the 707s plate (The Expanded Metal Company Limited, UK) had the greatest bubble removal ability because it had the large strand width and the second smallest open area. For a deeper understanding of the bubble removal effect, the real reaction surface area must be defined. Zhaolin Liu et al. [9] estimated the real surface area of platinum for the Pt/SWCNT and PtRu/SWCNT catalysts (A_{EL}) with cyclic voltammetry using the integrated charge in the hydrogen absorption region (Q_H). The areas (in m^2 g^{-1}) were calculated from the following formula, assuming a corresponding Pt loading value of 0.21 mC cm^{-2}:

$$A_{EL}(\text{m}^2\,\text{g}^{-1}\text{catalyst}) = \frac{Q_H}{0.21 \times 10^{-3}\text{Cgcatalyst}} \tag{4}$$

We used this formula to calculate the real surface area of the electrode and to study the increased area and fast bubble

* Corresponding author. Tel.: +886 3 5715131 34270; fax: +886 3 5733054.
E-mail addresses: chensl0701@yahoo.com.tw (S.-L. Chen), fangang@ess.nthu.edu.tw (F.-G. Tseng).

0378-7753/$ – see front matter © 2009 Elsevier B.V. All rights reserved.
doi:10.1016/j.jpowsour.2009.09.058

removal effect on the efficiency enhancement in the anode of a DMFC.

Yang et al. [10,11] adopted a CCD camera to observe the removal of carbon dioxide on the anode of a fuel cell and discussed the influence of current density, flow velocity and operating temperature on the efficiency of the cell. In addition, in situ visualization was also employed by Yang and Zhao [12] and Liao et al. [13] to investigate the relationship between CO_2 removal efficiency and cell performance. Zhang et al. [14] reported that uniform CO_2 bubbles of smaller size formed on hydrophilic anode GDL. Kulikovsky developed a simple model of the flow with gaseous bubbles in the anode channel of a DMFC. His model predicted a significant decrease in cell performance in regions with intense bubble formation [15,16]. However, few papers have discussed CO_2 gas behavior close to the catalyst surface. In our group, Zhuang et al. [17] reported different oxygen bubble removal abilities of Pt films on substrates with various supports in an H_2O_2 self-catalyzing reaction. Wang et al. [18] has found indirect electrochemical evidence of improved CO_2 removal ability by utilizing CNTs as a catalyst support in a DMFC anode. However, direct evidence is still not available.

In this paper, direct evidence of improved CO_2 removal efficiency by utilizing CNTs on carbon cloth (CNT/CC) as a Pt support is studied through direct bubble visualization and simultaneous electrochemical measurements of methanol oxidation. This study should be beneficial in the design of anode surfaces.

2. Experimental setup

In order to demonstrate the effects of highly efficient CO_2 bubble removal on CNT-supported nanocatalysts, we conducted three operations: electrode fabrication, electrochemical measurements (CV curve) and electrochemical measurements (I–t curve) with in situ bubble visualization.

2.1. Electrode fabrication process

The fabrication process of the three catalytic substrates for methanol oxidation testing is shown in Fig. 1. Three kinds of substrates were employed as catalyst supports for the CO_2 microbubble removal experiments, including carbon paper (CP), carbon cloth (CC) and CNTs grown on carbon cloth (CNT/CC). For CNT/CC, 30 nm Ti and 10 nm Ni were coated, in that order, by E-beam deposition on CC substrates. The CNTs were grown by metal catalyzed thermal chemical vapor deposition (CVD) with ethylene gas (C_2H_4) as the carbon source at 800 °C. After the growth of the CNTs, Pt nanoparticles were deposited by chemical reduction as the methanol catalyst layer on the CP, CC, and CNT/CC samples. In the catalyst deposition, a test sample with a 2 cm^2 open area was immersed in a 6 M H_2SO_4 aqueous solution at 80 °C for 1 h to modify the hydrophilic surface, and then in a solution of H_2PtCl_6, ethylene glycol (Eg) and 0.5 M NH_4OH at 160 °C for 1.5 h under supersonic vibration. After reduction, the sample was rinsed with deionized (DI) water and dried at 65 °C for 5 min. After the Pt chemical reduction process, Teflon was coated on the middle-right side of the sample (red circle in Fig. 1) to protect the current conduction area. A copper sheet was then attached to the right side of the sample for current conduction (green ellipse in Fig. 1).

2.2. Electrochemical measurements

Fig. 2 shows the schematic diagram of the setup for the simultaneous electrochemical detection and optical observations. By utilizing this system, the dynamic CO_2 microbubble detachment behavior and electrochemical I–t signal could be recorded coherently. A CHI model 760I potentiostat/galvanostat and a conventional three-electrode test cell, including a platinum coated

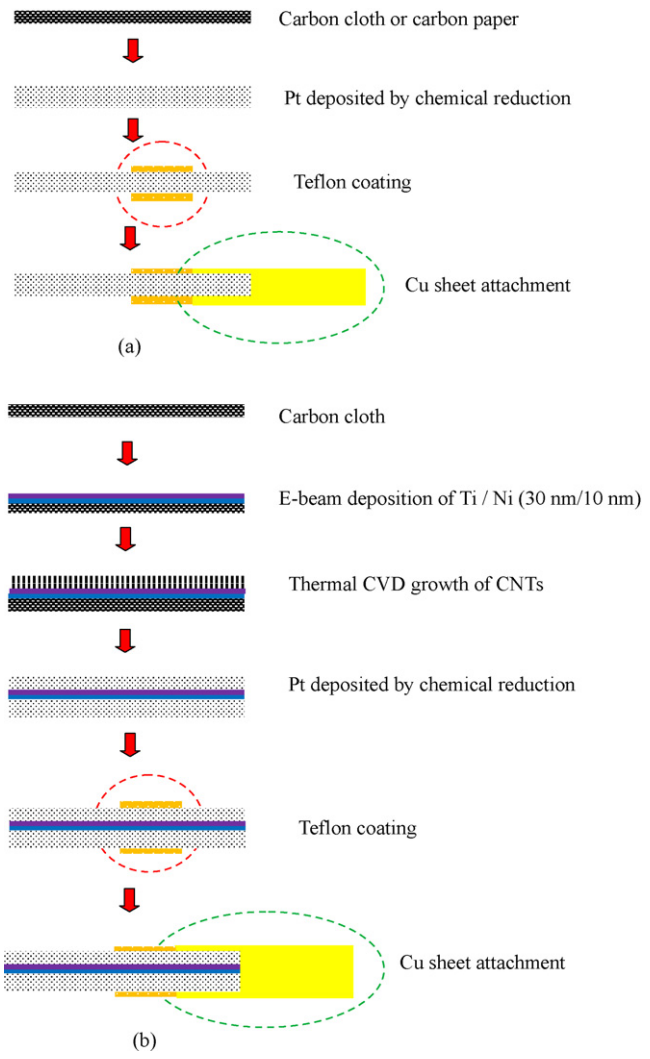

Fig. 1. Fabrication process of nano Pt catalysts on (a) CC or CP and (b) CNT/CC substrates for CO_2 microbubble removal experiments.

titanium net as a counter electrode, a saturated calomel reference electrode (SCE), and the sample acting as the working electrode, were used for the electrochemical measurements. The sample had a definite area of 1 cm^2 for CO_2 microbubble visualization. The electro-catalysis properties were measured by cyclic voltammetry (CV) in 0.5 M H_2SO_4 aqueous solutions (potential sweep range: −0.25 to 1 V, scan rate: 50 mV s^{-1}) and 1 M CH_3OH + 0.5 M H_2SO_4

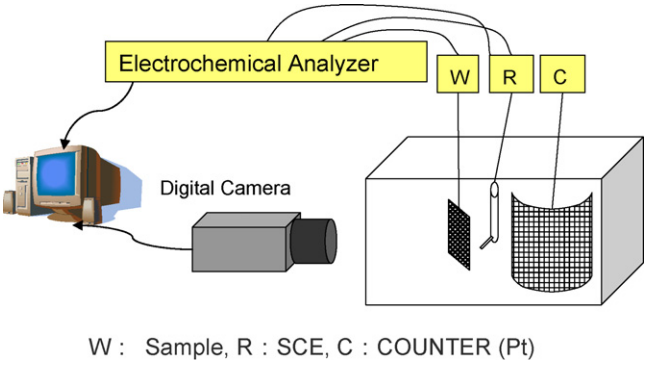

Fig. 2. Schematic diagram of the setup for in situ electrochemical detection and optical observation. (W: working electrode, sample; R: reference electrode, SCE; C: counter electrode, Pt-coated Ti net.).

aqueous solutions (potential sweep range: −0.2 to 0.9 V, scan rate: 20 mV s^{-1}), respectively. All experiments were carried out at either 20 or 40 °C with N_2 saturation at atmospheric pressure. All chemicals were reagent grade and DI water was used throughout the experiment.

3. Results and discussion

3.1. Electro-catalytic performance

Fig. 3(a)–(c) show the SEM images of the Pt nanoparticles chemically reduced on the CNT/CC, CP and CC substrates, respectively. The diameter of each support material was about 40–60 nm for the CNTs on carbon cloth, 7 μm for the fibers of carbon paper and 7.5 μm for the fibers of carbon cloth. The Pt catalyst layers were uniformly distributed on the CNT/CC, CP and CC samples, and the average size of Pt catalyst on the CNT/CC were around 3.77 nm, which is smaller than that of the Pt catalyst on the CP and CC samples (5.01 nm).

The real reaction surfaces per gram of the platinum catalysts for the Pt/CNT/CC, Pt/CP and Pt/CC samples (A_{EL}) were estimated by integrating the charge in the hydrogen absorption region (Q_H) in the cyclic voltammograms (hatched area in Fig. 4(a)). The areas (in $m^2\ g^{-1}$) were calculated by Eq. (4), assuming a corresponding Pt loading value of 0.21 mC cm^{-2}. As demonstrated by the results in Table 1, the Pt real surface per gram was, as expected, 73.7% higher on the CNT/CC-supported Pt catalyst (52.45 $m^2\ g^{-1}$) than on the CC-supported Pt catalyst (30.19 $m^2\ g^{-1}$). All measurements were made with the same catalyst loading method on a 1 cm × 2 cm rectangular electrode. The use of CNTs as the catalyst support caused significant differences in the Pt real surface area per gram. However, this difference was normalized in the comparisons among different samples that follows.

Fig. 4(a) shows the 5th cyclic voltammogram (CV) results of the catalytic reaction of the Pt catalyst on different carbon supports in 0.5 M H_2SO_4 at room temperature (20 °C) under a saturated N_2 atmosphere. The sweeping range was from −0.25 to 1 V (vs. SCE) and the sweeping rate was 50 mV s^{-1}. The areas of the hydrogen adsorption were CNT/CC > CP > CC, which may be due to a larger surface area and a larger hydrogen proton adsorption created by the CNT/CC electrode.

The methanol electro-catalytic capability of Pt/CNT/CC, Pt/CP and Pt/CC were examined by cyclic voltammetry in 1 M CH_3OH + 0.5 M H_2SO_4 aqueous solutions, as shown in Fig. 4(b). Two oxidation peaks in the cyclic voltammogram were observed, and they corresponded to the oxidation of methanol and the oxidation of carbon monoxide, with potential ranges of 0.62–0.64 V and 0.45–0.48 V, respectively. The electro-catalytic properties of the Pt film in 1 M CH_3OH + 0.5 M H_2SO_4 aqueous solutions were characterized by the peak current density and peak potential from the oxidation of methanol by cyclic voltammetry. A higher peak current (I_p) (170 mA) was found for the Pt/CNT/CC electrode, because of the combined benefits of a larger reaction surface and the better CO_2 microbubble removal capability provided by the CNTs.

Fig. 4(c) shows the omit-area-effect CV curve of Fig. 4(b). The current was divided by the real reactive surface area per gram of catalyst (A_{EL}) to deduce the reaction area effect. Fig. 4(d) compares the peak current (left figure) and the omit-area-effect (right figure) of methanol oxidation for the three substrates. From the right figure of Fig. 4(d), CP and CC have almost the same omit-area-effect

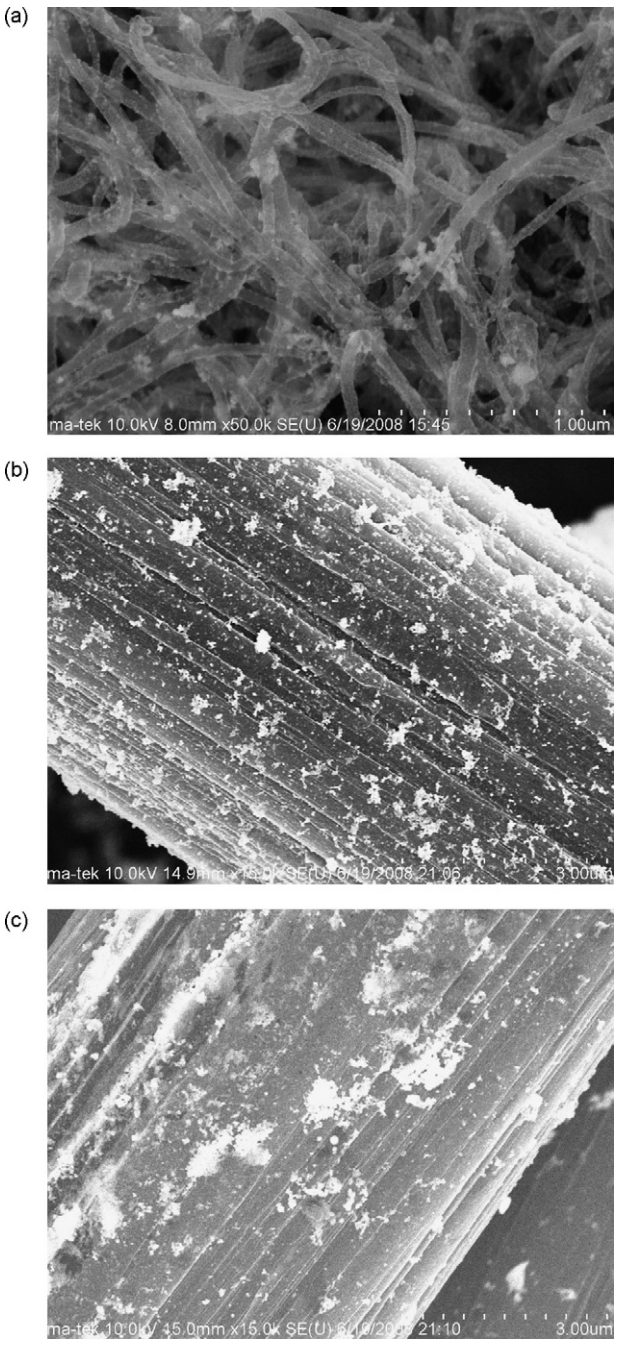

Fig. 3. SEM images of reduced Pt nanoparticles on (a) CNT/CC, 50,000× (b) CP, 15,000× and (c) CC, 15,000×.

Table 1
Real (active) surface areas of Pt/CNT/CC, Pt/CP and Pt/CC catalysts as determined by hydrogen electro-adsorption.

Origin of Pt/C catalyst	Q_H [a] (mC)	S_{EL} [b] (cm^2)	Catalyst loading (mg cm^{-2})	A_{EL} [c] ($m^2\ g^{-1}$ catalyst)	Onset potential (V)
Pt/CNT/CC	35.2	167.4	0.319	52.45	0.37
Pt/CP	25.6	121.7	0.299	40.76	0.42
Pt/CC	10.7	50.9	0.169	30.19	0.42

[a] Q_H: charges exchanged during the electro-adsorption of hydrogen on Pt.
[b] S_{EL}: real surface area obtained electrochemically.
[c] A_{EL}: real surface area obtained electrochemically per gram of catalyst.

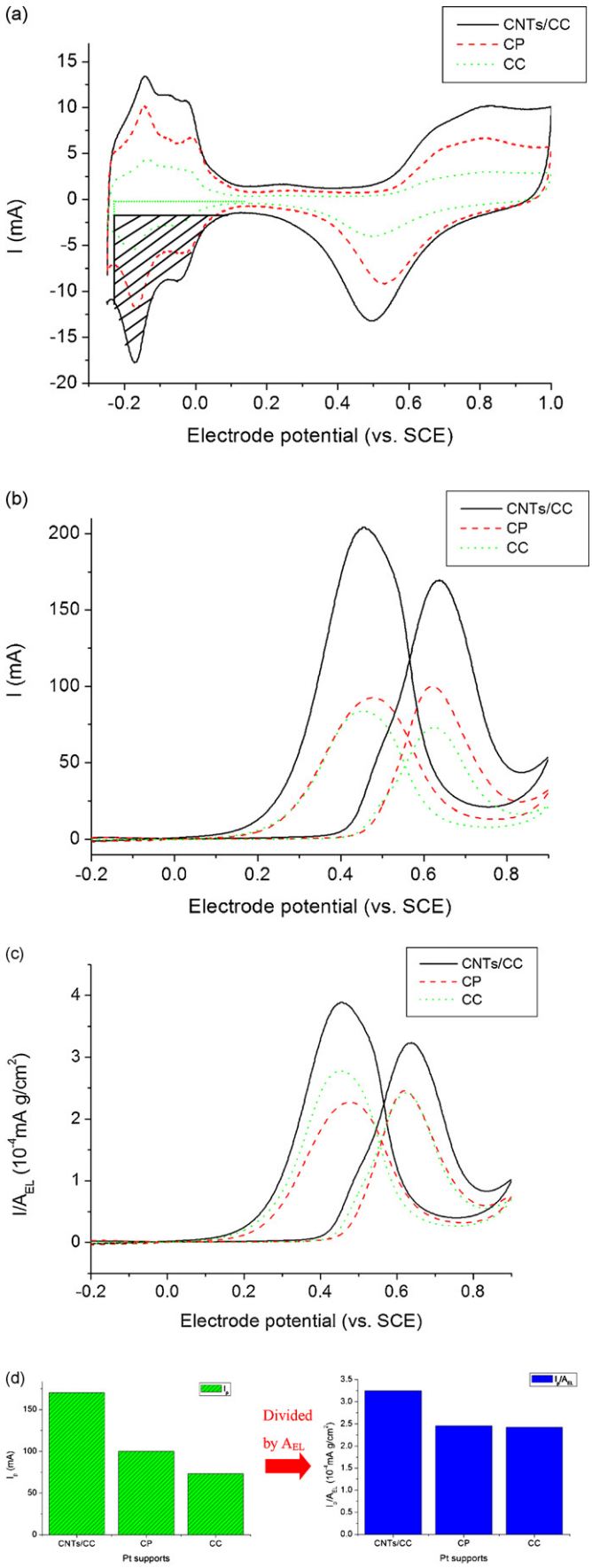

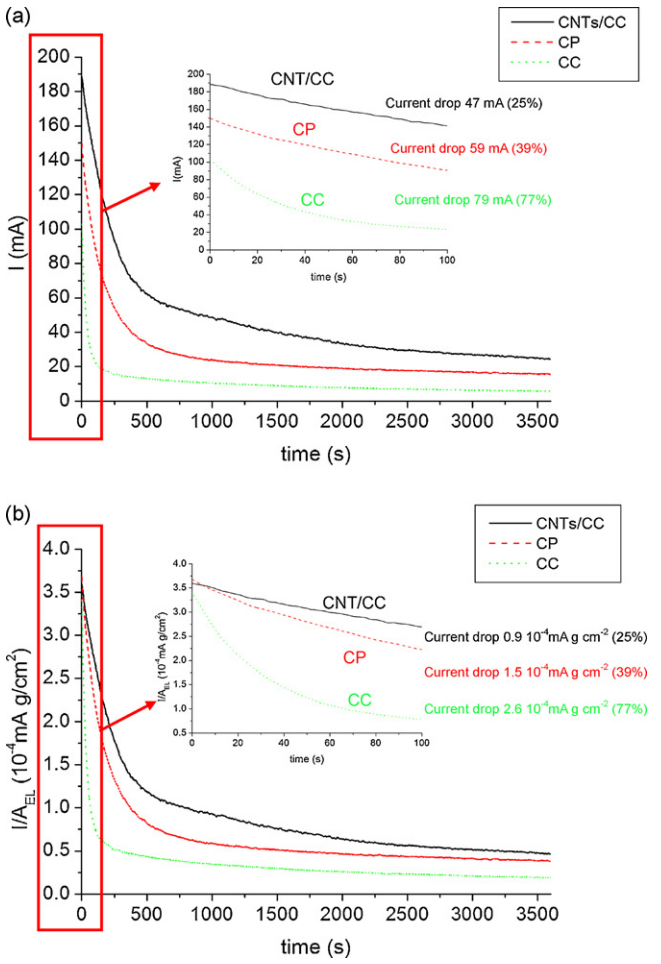

Fig. 5. (a) Current to time (I–t) curve, (b) current divided by A_{EL} to time (I/A_{EL}–t) curve of the Pt/CNT/CC, Pt/CP and Pt/CC electrodes at 0.6 V (vs. SCE) in N_2 saturated 1 M CH_3OH + 0.5 M H_2SO_4 aqueous solutions at 40 °C over 3600 s.

peak current density, but CNT/CC had a significantly larger one after dividing the real reaction surface area, suggesting an enhanced peak current density coming from the CNTs' rapid CO_2 microbubble removal capability.

Effect of electrochemical activity of the Pt/CNT/CC, Pt/CP and Pt/CC catalytic surfaces can be shown as Table 2. The current per Pt loading weight, $i_p \times A_{EL}$, of the Pt/CNT/CC catalyst was 89,165 A g^{-1}, which is 4 times higher than the Pt/CC catalyst. This is because the Pt/CNT/CC has larger reaction surface area. Current per real active surface area can be calculated as $I_p \times 2/S_{EL}$, in which geometrical surface area of electrode is 2 cm^2 (two sides). The current per real active surface area of the Pt/CC catalyst was 2868 A cm^{-2}, it is the largest of these three types substrate because of the small electrode area of Pt/CC, which may be due to the large particle size of Pt deposited on CC. The current per real surface per gram of Pt catalyst, I_p/A_{EL}, of the Pt/CNT/CC catalyst was 3.2412×10^{-4} mA g cm^{-2}, which is the largest among three different type substrates. For comparison purpose, we defined three new parameters, including the total performance enhancement ratio $E_{T\text{-}CNTs}$, the enhancement

Fig. 4. Cyclic voltammograms for CNT/CC, CP and CC samples with chemically reduced Pt in (a) 0.5 M H_2SO_4 aqueous solutions with N_2 saturation, (b) 1 M CH_3OH + 0.5 M H_2SO_4 aqueous solutions with N_2 saturation, (c) 1 M CH_3OH + 0.5 M H_2SO_4 aqueous solutions with N_2 saturation divided by A_{EL}, (d) I_p and I_p/A_{EL} for different electrodes. The sweeping rate of the CV was 50 and 20 mV s^{-1} for 0.5 M H_2SO_4 aqueous solutions and 1 M CH_3OH + 0.5 M H_2SO_4 aqueous solutions, respectively, and the room temperature was at 20 °C.

Table 2
Effect of electrochemical activity of the Pt/CNT/CC, Pt/CP and Pt/CC catalytic surfaces.

Origin of Pt/C catalyst	I_p[a] (mA)	S_{EL} (cm^2)	A_{EL} ($m^2\,g^{-1}$)	$i_p \times A_{EL}$[b] ($A\,g^{-1}$)	$I_p \times 2/S_{EL}$[c] ($A\,cm^{-2}$)	I_p/A_{EL}[d] (10^{-4} mA g cm^{-2})	E_T[e]	E_A[f]	E_B[g]
Pt/CNT/CC	170	167.4	52.45	89,165	2,031	3.2412	2.329	1.737	1.340
Pt/CP	100	121.7	40.76	40,760	1,643	2.4534	1.370	1.350	1.015
Pt/CC	73	50.9	30.19	22,039	2,868	2.4180	1	1	1

[a] I_p: peak current of the electrode.
[b] $i_p \times A_{EL}$: peak current per Pt loading weight of the electrode.
[c] $I_p \times 2/S_{EL}$: peak current per real active surface area of the electrode.
[d] I_p/A_{EL}: peak current per real surface per gram of Pt catalyst of the electrode.
[e] E_T: total performance enhancement ratio for CNTs, CP, CC toward CC.
[f] E_A: enhancement ratio of the reaction area increment for CNTs, CP, CC toward CC.
[g] E_B: enhancement ratio of the bubble removal rate for CNTs, CP, CC toward CC.

ratio due to the reaction area increment $E_{A\text{-}CNTs}$, and the enhancement ratio of the bubble removal rate $E_{B\text{-}CNTs}$. The total performance enhancement ratio $E_{T\text{-}CNTs}$ for CNTs toward CC ($E_{T\text{-}CNTs} = I_{p\text{-}CNT}/I_{p\text{-}CC}$) can be expressed as the product of the enhancement ratio due to the reaction area increment $E_{A\text{-}CNTs}$ ($= A_{EL\text{-}CNT}/A_{EL\text{-}CC}$) and the enhancement ratio of the bubble removal rate $E_{B\text{-}CNTs}$:

$$(E_{T\text{-}CNTs}) = (E_{A\text{-}CNTs})(E_{B\text{-}CNTs}) \quad (5)$$

As illustrated in Table 2, $E_{T\text{-}CNTs}$ and $E_{A\text{-}CNTs}$ are equal to 2.329 and 1.737, respectively. As a result, the $E_{B\text{-}CNTs}$ can be estimated as 1.340, meaning that the 34% performance enhancement achieved is due to the faster bubble removal rate. If we calculate similar parameters for the CP case, we find that $E_{T\text{-}CP}$ and $E_{A\text{-}CP}$ are equal to 1.370 and 1.350, respectively. As a result, the $E_{B\text{-}CP}$ can be estimated as 1.015, meaning that there is only a 1.5% enhancement due to bubble removal for CP. This comparison can provide a quick estimation of how CNTs can aid bubble removal and the performance of the peak current.

Electrochemical I–t curves were also utilized to qualitatively compare the CO_2 microbubble detachment capability. Under diffusion control according to the Cottrell equation (Eq. (6)), the current $I(t)$ is proportional to the electrode real surface area per gram of catalyst A_{EL} [19].

$$I(t) = I_d(t) = \frac{(nFA_{EL}{D_0}^{1/2}{C_0}^*)}{(\pi^{1/2}t^{1/2})} \quad (6)$$

where n is the charge number, I_d is the diffusion limited current, F is the Faraday constant, A_{EL} is the electrode real surface area per gram of catalyst, D_0 is the diffusion coefficient and $C_0(x, 0) = C_0^*$

The electrochemical reaction equation of the anodic CH_3OH system is shown in Eq. (1). Methanol combines with water to form carbon dioxide gas, six protons and six electrons. Fig. 5(a) shows the relationship between the reaction current and time (I–t) over 3600 s by applying 0.6 V (SCE) to the reaction electrode in the methanol solution. The reaction reached diffusion control within 2500 s, as seen in Fig. 5. At diffusion control, the Pt/CNT/CC sample had a larger current and smaller current drop (47 mA, 25%) than the Pt/CP sample (59 mA, 39%) and the Pt/CC sample (79 mA, 77%). When the current was normalized by the real reaction area per gram of catalyst A_{EL}, as shown in Fig. 5(b), the normalized start-up current ($(3.3–3.7) \times 10^{-4}$ mA g cm^{-2}) became almost identical. However, the current drop rates were still different, and the Pt/CNT/CC sample had a smaller current drop rate (0.9×10^{-4} mA g cm^{-2}, 25%) than the Pt/CP sample (1.5×10^{-4} mA g cm^{-2}, 39%) or the Pt/CC sample

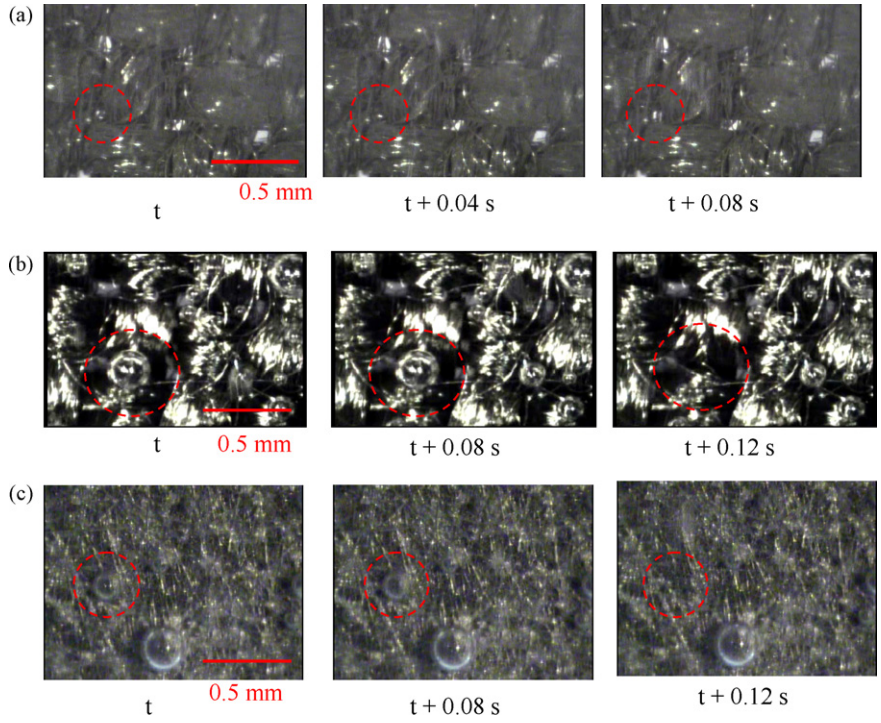

Fig. 6. The in situ bubble images captured at $t = 99$ s for (a) Pt/CNT/CC, (b) Pt/CC and (c) Pt/CP electrodes at 0.6 V (vs. SCE) in N_2 saturated 1 M CH_3OH + 0.5 M H_2SO_4 aqueous solutions at 40 °C.

(2.6×10^{-4} mA g cm^{-2}, 77%). The smaller current drop in the CNTs sample can be attributed to the lower bubble coverage ratio on the electrode.

3.2. Comparison of bubble detaching ability

To verify the above hypothesis by indirect electrochemical characteristics, direct visualization of the bubble removal rates on different electrode surfaces was carried out. The in situ images were captured at t = 99 s for Pt/CNT/CC, Pt/CC, and Pt/CP at 0.6 V (vs. SCE) in an N_2 saturated 1 M CH_3OH + 0.5 M H_2SO_4 aqueous solution at 40 °C, as shown in Fig. 6(a)–(c), respectively. In Fig. 6(a), the Pt/CNT/CC electrode, smaller CO_2 microbubbles were observed compared with those on the Pt/CC and Pt/CP electrodes, and they detached more easily. These CO_2 microbubble diameters were around 20–40 μm, and one of the typical bubbles, circled in red in Fig. 6(a), had a diameter of 33 μm. At t + 0.04 s, this CO_2 microbubble grew to a diameter of 38 μm and was ready to detach. In Fig. 6(b), the Pt/CC electrode, larger CO_2 microbubbles (100–220 μm) were observed with higher adhesion force to the electrode surface, and one of them, circled in red, had a diameter of 205 μm. This bubble detached at t + 0.08 s, which was longer than those on the Pt/CNT/CC electrode. A similar result was observed on the Pt/CP electrode, with a bubble detaching at t + 0.08 s, but smaller bubble detachment diameters of around 30–100 μm were observed in this case.

Statistical analysis of the images is shown in Fig. 7. As can be seen in Fig. 7(a), the Pt/CNT/CC electrode had a smaller CO_2 microbubble detachment diameter (27.4 μm) compared with the Pt/CP and Pt/CC electrodes, which had bubble detachment diameters of 58.7 μm and 173 μm, respectively. Fig. 7(b) shows that

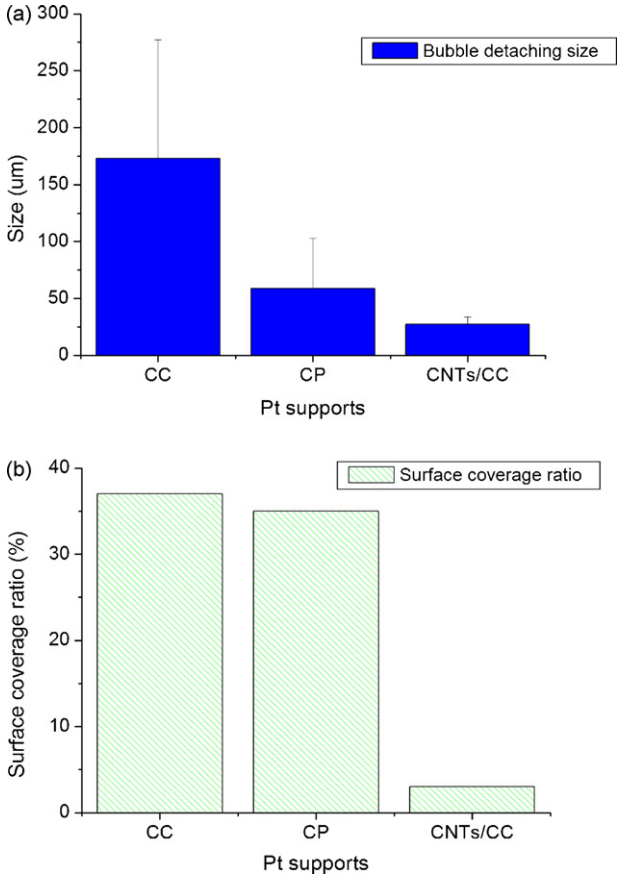

Fig. 7. (a) The bubble detachment size and (b) bubble surface coverage ratio on Pt/CC, Pt/CP and Pt/CNT/CC electrodes by applying 0.6 V (vs. SCE) in a 1 M CH_3OH + 0.5 M H_2SO_4 aqueous solution at 40 °C.

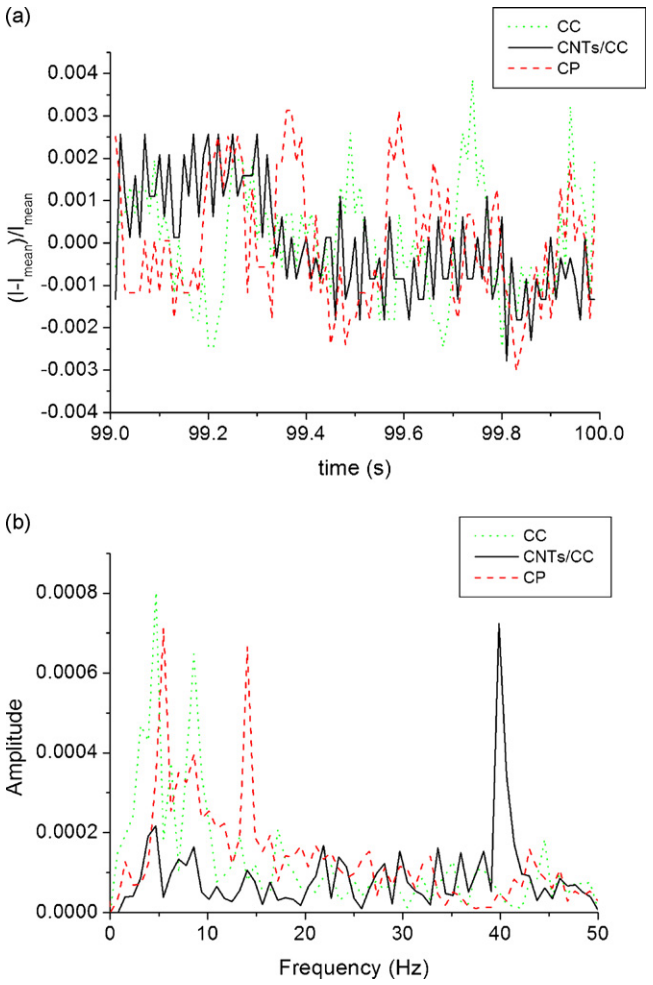

Fig. 8. (a) $(I - I_{mean})/I_{mean}$ to time curve from t = 99 to 100 s. (b) Fast Fourier transform of the vibration curve from t = 99 to 100 s for the Pt/CNT/CC, Pt/CP and Pt/CC electrodes at 0.6 V (vs. SCE) in N_2 saturated 1 M CH_3OH + 0.5 M H_2SO_4 aqueous solutions at 40 °C.

the coverage ratios of the reaction surface on different electrodes were 3%, 35% and 37% for the Pt/CNT/CC, Pt/CP, and Pt/CC electrodes, respectively. As a result, the uncovered reaction area on the Pt/CNT/CC electrode was 32% and 34% higher than on the Pt/CP and Pt/CC electrodes, respectively, which agrees with the estimation of the E_B from the previous discussion.

For detailed analysis of the current vibration phenomenon, the vibration time sequence was expanded between 99 and 100 s, and the sampling rate was 100 points per second, as shown in Fig. 8(a). The fast Fourier transform (FFT) results are shown in Fig. 8(b). From Fig. 8(a), we found that the Pt/CNT/CC electrode had a higher frequency current vibration than the Pt/CC and Pt/CP electrodes. The Pt/CNT/CC electrode also had smaller current amplitude than the Pt/CC and Pt/CP electrodes. The FFT results show that the Pt/CNT/CC electrode had an obvious peak at 39.8 Hz, but the Pt/CC electrode had a lower frequency distribution, with peaks at 4.7 and 8.6 Hz, respectively, while the Pt/CP electrode also had a lower frequency distribution, with peaks at 5.5 and 14 Hz, respectively. The higher vibration frequency for the Pt/CNT/CC electrode also suggested smaller bubble generation and faster detachment.

4. Conclusion

In the present study, it is concluded that electrodes with CNTs as catalyst support can directly limit CO_2 microbubble growth in

electrochemical catalytic reactions and lead to improvement of the CO_2 microbubble detaching capability. This rapid CO_2 microbubble removal behavior is directly related to the high frequency current vibration. Also, the high bubble detachment rate and smaller detachment size observed in the optical system are consistent with the high frequency of current vibration in the electrochemical system. These results demonstrate that electrodes with nanostructures contribute to the mass transfer for electro-catalytic reactions composed of liquid reactants and gaseous products. The higher CO_2 microbubble detachment rate on Pt/CNT/CC helps create more catalytic sites, thus promoting higher electrochemical reaction currents, leading to a higher frequency current fluctuation. The uncovered reaction area on the Pt/CNT/CC electrode was 34%, and was 32% higher than that on the Pt/CC and Pt/CP electrodes, respectively, which equates to a 34% and 32% performance enhancement, respectively, in the CNT-modified electrodes (Pt/CNT/CC) due to a faster CO_2 bubble removal capability.

Acknowledgements

The authors would like to thank the National Science Council of the Republic of China, Taiwan, for financially supporting this research under Contract No. NSC 97-2623-7-007-012-ET, and the Department of Economy, Taiwan, ROC for project support.

References

[1] C.K. Dyer, J. Power Sources 106 (2002) 31–34.
[2] A. Heinzel, C. Hebling, M. Muller, M. Zedda, C. Muller, J. Power Sources 105 (2002) 250–255.
[3] T. Schultz, Su Zhou, Kai Sundmacher, Chem. Eng. 24 (2001) 12.
[4] R. Dillon, S. Srinivasan, A.S. Arico, V. Antonucci, J. Power Sources 127 (2004) 112–126.
[5] K. Scott, W.M. Taama, P. Argyropoulos, J. Appl. Electrochem. 28 (1998) 1389–1397.
[6] G.Q. Lu, C.Y. Wang, J. Power Sources 134 (2004) 33–40.
[7] T. Bewer, T. Beckmann, H. Dohle, J. Mergel, D. Stolten, J. Power Sources 125 (2004) 1–9.
[8] K. Scott, P. Argyropoulos, P. Yiannopoulos, W.M. Taama, J. Appl. Electrochem. 31 (2001) 823–832.
[9] Z. Liu, X.Y. Ling, B. Guo, L. Hong, J.Y. Lee, J. Power Sources 167 (2007) 272–280.
[10] H. Yang, T.S. Zhao, Q. Ye, Electrochem. Commun. 6 (2004) 1098–1103.
[11] H. Yang, T.S. Zhao, Q. Ye, J. Power Sources 139 (2005) 79–90.
[12] H. Yang, T.S. Zhao, Electrochim. Acta 50 (2005) 3243–3252.
[13] Q. Liao, X. Zhu, X.Y. Zheng, Y.D. Ding, J. Power Sources 171 (2007) 644–651.
[14] J. Zhang, G.P. Yin, Q.Z. Lai, Z.B. Wang, K.D. Cai, P. Liu, J. Power Sources 168 (2007) 453–458.
[15] A.A. Kulikovsky, Electrochem. Commun. 7 (2005) 237–243.
[16] A.A. Kulikovsky, Electrochim. Acta 51 (2006) 2003–2011.
[17] R.X. Zhuang, F.G. Tseng, Y.S. Wu, S.K. Wang, The 22nd National Conference on Mechanical Engineering (Tauyoun, Taiwan, 25 November 2005) E7–005.
[18] S.K. Wang, F.G. Tseng, T.K. Yeh, C.C. Chieng, J. Power Sources 167 (2007) 413–419.
[19] J. Wang, Anal. Electrochem. 2 (2001) 60–67.